cyanate has a pronounced effect on the oxygen binding step, and chloride effects mainly the subsequent redox steps.

The rate constant for the binding of O_2 is fairly insensitive to the presence of anions. The values of k_f for the three species in Table VI differ only by a factor of ~4. This is somewhat surprising, since one might have expected that differences in oxygen affinity would be reflected in the kinetics of both forward and reverse reactions.

The effect on the release of O_2 is much more pronounced. The rate constant k_r is the largest for the aquo complex, intermediate for the chloro, and too small to observe for the thiocyanato. The electronic structure of these cobalt-oxygen adducts is probably best considered intermediate between $Co^{II}-O_2$ and $Co^{III}-O_2^-$.[1e,5] The latter structure should be stabilized the most by the most strongly coordinated anion, SCN^-, and thus the dissociation to O_2 and cobalt(II) should be least favorable for $(SCN)L^2CoO_2^+$, as experimentally observed. The high equilibrium constant for the binding of O_2 might be partly responsible for the accelerated autoxidation of L^2Co^{2+} in the presence of SCN^-. Subsequent redox steps were not investigated, but they are probably affected too, as judged from the results obtained in the presence of chloride.

The equilibrium constant for the binding of O_2 by $(Cl)L^2Co^+$, 560 M^{-1}, is not much larger than that for the uncomplexed L^2Co^{2+}, 301 M^{-1}. Both the forward and reverse reactions are somewhat faster for L^2Co^{2+} than for $(Cl)L^2Co^+$. Despite that, the irreversible oxidation of L^2Co^{2+} is much faster in the presence of Cl^-, demonstrating that the redox steps following reaction 16 must be accelerated by Cl^-. Similar conclusions have been reached earlier for some other cobalt complexes.[3,4] We have also observed that Br^- accelerates dramatically the autoxidation of L^2Co^{2+}, although it has no effect on the oxygen binding step. This is also consistent with strong catalysis in the redox steps. A detailed study of these reactions is in progress.

Acknowledgment. This research was supported by the U.S. Department of Energy, Office of Basic Energy Sciences, Chemical Sciences Division, under Contract W-7405-Eng-82. We are grateful to S. Lee for the synthesis of the macrocyclic ligand and to Dr. Lee Daniels of the Iowa State University Molecular Structure Laboratory for the crystal structure determination.

Registry No. $(Cl^-)L^2Co^+$, 126543-76-8; $(SCN^-)L_2Co^+$, 126543-77-9; $[Co(C\text{-}meso\text{-}Me_6[14]aneN_4)(ClO_4)_2]$, 126543-78-0.

Supplementary Material Available: Tables of positional parameters for hydrogen atoms and general displacement parameter expressions (5 pages); a listing of observed and calculated structure factors (8 pages). Ordering information is given on any current masthead page.

Contribution from the Department of Chemistry, Stanford University, Stanford, California 94305

Variable-Energy Photoelectron Spectroscopic Comparison of the Bonding in Ferric Sulfide and Ferric Chloride: An Alternative Description of the Near-IR-Visible Spin-Forbidden Transitions in High-Spin d^5 Complexes

Kristine D. Butcher, Matthew S. Gebhard, and Edward I. Solomon*

Received September 25, 1989

Variable photon energy, valence-band, and core-level photoelectron spectroscopy (PES) have been used to determine the electronic structure and bonding in tetrahedral high-spin d^5 FeS_4^{5-}. The valence-band PES spectra over the range 25-100 eV show strong similarities with our previous results on tetrahedral $FeCl_4^-$. The three-peak pattern and their energy splittings and intensity ratios all parallel the data on $FeCl_4^-$. Also, as in ferric chloride, the major resonance enhancement appears in the deepest binding energy portion of the main band, indicating that dominant metal character is present in the bonding levels at deepest binding energy. No off-resonance PES intensity is observed in the satellite, indicating that little relaxation occurs upon ionization. These results demonstrate that the ground-state electronic structure of ferric sulfide parallels that of ferric chloride and is inverted from the normal description for transition-metal complexes, which places the dominant metal character in the antibonding levels at lowest binding energy. This inverted bonding scheme results from the large spin-polarization effects present in high-spin d^5 complexes. Analysis of the Fe 2p core level PES spectra allows a comparison of the covalency of tetrahedral ferric chloride and sulfide. The difference is relatively small and is due to the lower ionization energy of the sulfide relative to the chloride ligands. Alternatively, there is a large difference observed between the bound-state optical absorption spectra of ferric chloride relative to the sulfide (and thiolate) complex, which is not satisfactorily accounted for by ligand field theory but is explained by spin-unrestricted $X\alpha$ calculations. These studies indicate that the lowest energy spin-forbidden transitions in high-spin d^5 complexes, which are normally described as $d \rightarrow d$ transitions in ligand field theory, have extensive ligand-to-metal charge-transfer character.

I. Introduction

Our previous work has focused on determining the electronic structure and bonding in high-spin tetrahedral ferric chlorides as a first step toward understanding iron-sulfur active sites in proteins such as rubredoxin.[1] Theoretical studies of model iron thiolate complexes indicate that the ground-state bonding description of these iron-sulfur systems is inverted, with the HOMO exhibiting mostly ligand character and the metal character contained in the bonding levels at deeper binding energy.[2] This inverted ground state is also predicted for $FeCl_4^-$ and was experimentally confirmed by using variable-energy photoelectron spectroscopy (PES).[1d] The energy level diagram for the high-spin d^5 system including exchange can be depicted schematically as in Figure 1. The ground-state spin-unrestricted $X\alpha$ calculations indicate that the stabilization of the d levels is due to the large exchange interaction in high-spin d^5, which lowers the energy of the occupied $d\uparrow$ orbitals relative to the empty $d\downarrow$ orbitals.[3] The exchange splitting between ligand $\uparrow$ and $\downarrow$ levels is small, while the exchange in the Fe 3d levels is large and is present in the free-ion ^6S ground state. This exchange splitting is the greatest for the d^5 configuration and is sufficient to drop the $3d\uparrow$ levels below the ligand 3p valence levels. Both the $d\uparrow$ and $d\downarrow$ orbitals interact with the ligand 3p valence orbitals, resulting in a complex bonding scheme that contains dominant ligand character in both the spin-down bonding and

(1) (a) Deaton, J. C.; Gebhard, M. S.; Koch, S. A.; Millar, M.; Solomon, E. I. *J. Am. Chem. Soc.* **1988**, *110*, 6241. (b) Gebhard, M. S.; Deaton, J. C.; Koch, S. A.; Millar, M.; Solomon, E. I. *J. Am. Chem. Soc.*, in press. (c) Deaton, J. C.; Gebhard, M. S.; Solomon, E. I. *Inorg. Chem.* **1989**, *28*, 877. (d) Butcher, K. D.; Didziulis, S. V.; Briat, B.; Solomon, E. I. *J. Am. Chem. Soc.*, in press.

(2) (a) Norman, J. G., Jr.; Jackels, S. C. *J. Am. Chem. Soc.* **1975**, *97*, 3833. (b) Norman, J. G., Jr.; Ryan, P. B.; Noodleman, L. *J. Am. Chem. Soc.* **1980**, *102*, 4279. (c) Bair, R. A.; Goddard, W. A., III. *J. Am. Chem. Soc.* **1978**, *100*, 5669.

(3) The spin-unrestricted formalism allows different orbitals for different spins, thus splitting the d orbitals into occupied spin-up and unoccupied spin-down.

0020-1669/90/1329-2067$02.50/0

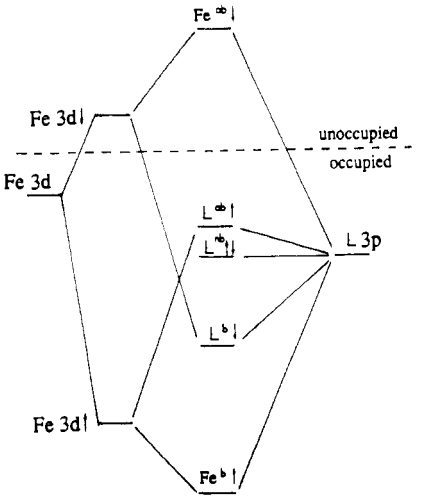

Figure 1. High-spin d^5 energy level diagram including the effects of exchange.

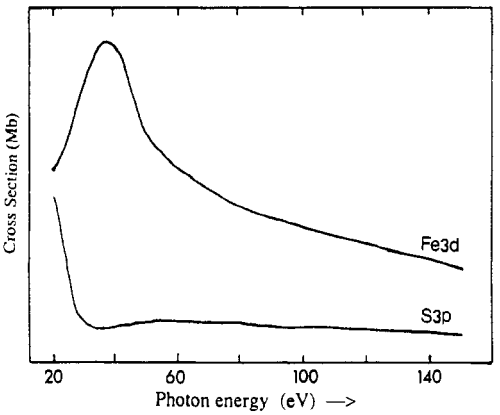

Figure 2. Atomic subshell photoionization cross sections for Fe 3d and S 3p as a function of photon energy, adapted from ref 7a.

spin-up antibonding levels. The LUMO remains mostly metal 3d as would be the case for a normal bonding scheme, but the HOMO is mostly ligand in character. While these calculations indicate that ferric chloride and ferric thiolate exhibit the same inverted ground state, quantitative differences in bonding must exist. Ferric thiolate complexes are more stable than their ferric chloride counterparts and in particular exhibit unusual optical absorption spectra with very low energy spin-forbidden transitions (interpreted as d → d) in the thiolate relative to the chloride.[1a-c] In terms of a ligand field theory (LFT) description the low energy of the spin-forbidden transitions would require a drastic reduction in electron repulsion due to increased covalency associated with the sulfur ligation.[1a,b]

In this study we focus on the related ferric sulfide[4] as the PES spectra are not complicated by photoemission from the R group or the organic counterion present in the ferric thiolate complexes. Xα–SW calculations[5] indicate a great deal of similarity in bonding between these two systems, as does the similarities in their charge-transfer spectra.[1,5] In addition, a weak low energy (7500 cm^{-1}) absorption feature has been observed[6] in the $KFeS_2$ compound. This feature occurs at approximately the same energy as the spin-foribdden "d → d" transition in the mononuclear ferric tetrathiolate complex. Our PES study on $FeCl_4^-$ is extended here to high-spin tetrahedral FeS_4^{5-} in order to experimentally determine if the inverted bonding scheme is in fact present in the sulfide, to define quantitative differences in bonding between these two systems, and to use these differences to obtain insight into the striking absorption spectral differences between the $FeCl_4^-$ and $Fe(SR)_4^-$ complexes. Further, a description of these absorption transitions based on the inverted bonding scheme in Figure 1 is developed that is compared to the traditional ligand field theory interpretation.

The changes in peak intensity with input photon energy (using synchrotron radiation) are exploited in order to make a detailed assignment of the valence-band PES features. The photoionization cross section, σ, exhibits two features of interest:[7] (1) the general changes in σ with input photon energy and (2) resonance effects, which involve initial excitation into bound states. The cross sections for Fe 3d and S 3p, obtained from ref 3a, are reproduced in Figure 2. In general, metal 3d cross sections show a broad, delayed intensity maximum peaking in the photon energy region 40–50 eV, while the S 3p cross section peaks near threshold and then decreases with increasing photon energy.[7] The S 3p cross section additionally exhibits a local intensity minimum near 35–40 eV due to the node in the 3p radial wave function.[8]

The valence-band PES peak intensities are also affected by the presence of resonance at the metal 3p absorption edge. The resonance process, defined by Davis,[9] is given in Scheme I. At the absorption edge, a metal 3p electron is excited into the metal 3d level. This excited state autoionizes through a super-Coster–Kronig (SCK) Auger decay process, resulting in a $|d^4\rangle$ final state, which is the same as that reached by direct d ionization. The autoionization process is responsible for the resonance intensity and has a very high probability due to the localized nature and large repulsion of the d electrons. Thus, the presence of resonance in PES features provides a sensitive probe of the final-state metal $|d^4\rangle$ character in the PES peaks.

Scheme I

d ionization: $3p^63d^5 \rightarrow 3p^63d^4$

resonance: $3p^63d^5 \rightarrow 3p^53d^6 \rightarrow 3p^63d^4$

PES studies on $CuCl_4^{2-}$ demonstrated the importance of including the effects of relaxation in the analysis of PES spectra.[10] Dramatic changes in the wave functions may occur on ionization due to the relaxation of orbitals in order to minimize the large change in metal-centered electron repulsion accompanying ionization. As a result of this relaxation, intensity is shifted into deeper binding energy satellite peaks.[11] The satellite peak corresponds to the simultaneous ionization plus shake-up of a second electron to create an excited final state (Scheme II). This two-electron transition is formally forbidden and should have no intensity. Final-state relaxation allows intensity to be shifted from the lowest energy final state to the excited final state provided that the shake-up involves a level of the same symmetry as the one-electron ionized level.[12] The principal ionization can involve

(4) It should be noted that $KFeS_2$ is an infinite-chain semiconductor thus having some energy dispersion in its band structure. This dispersion will broaden the PES spectrum relative to that of mononuclear ferric sulfide and thiolate. Band structure calculations[28] on the related $CuFeS_2$ infinite lattice compound indicate that the Fe(III) 3d orbital dispersion is small with the S^{2-} 3p orbital dispersion being greater. These calculations indicate that the qualitative energy order of the bands is unchanged on going from the mononuclear FeS_4^{5-} cluster to the extended lattice.

(5) Taft, C. A.; Braga, M. *Phys. Rev. B: Condens. Matter.* **1980**, *21*, 5802. Note: Taft and Braga used tangent spheres in their calculations, which leads to considerable charge density remaining in the intersphere region. In addition, repartitioned wave functions were not reported, so the values for metal character quoted represent a minimum estimate.

(6) Schmidtke, H.-H.; Packroff, R.; Bronger, W.; Muller, P. *Chem. Phys. Lett.* **1988**, *150*, 129.

(7) (a) Yeh, J. J.; Lindau, I. *At. Data Nucl. Data Tables* **1985**, *32*, 1. (b) Fano, U.; Cooper, J. W. *Rev. Mod. Phys.* **1968**, *40*, 441. (c) Manson, S. T.; Cooper, J. W. *Phys. Rev.* **1968**, *165*, 126. (d) Eastman, D. E.; Kusnietz, M. *J. Appl. Phys.* **1971**, *42*, 1396.

(8) Cooper, J. W. *Phys. Rev.* **1962**, *128*, 681.

(9) (a) Davis, L. C. *Phys. Rev. B: Condens. Matter.* **1982**, *25*, 2912. (b) Davis, L. C.; Feldkamp, L. A. *Phys. Rev. B: Condens. Matter.* **1981**, *23*, 6239.

(10) Didziulis, S. V.; Cohen, S. L.; Gewirth, A. A.; Solomon, E. I. *J. Am. Chem. Soc.* **1988**, *110*, 250.

(11) (a) Frost, D. C.; Ishitani, A.; McDowell, C. A. *Mol. Phys.* **1972**, *24*, 861. (b) van der Laan, G. *Solid State Commun.* **1982**, *42*, 165. (c) Thuler, M. R.; Benbow, R. L.; Hurych, Z. *Phys. Rev. B: Condens. Matter.* **1982**, *26*, 669.

a valence electron level as discussed above or a core level (in this study the Fe $2p_{3/2}$ at 711 eV). In the case of valence ionization, the additional metal 3d hole–hole Coulomb repulsion, U, is responsible for the relaxation and accompanying valence satellite intensity. For core ionization, the 2p–3d Coulomb interaction, Q, produces the relaxation.[13] The valence relaxation is smaller than the core relaxation and has been estimated as $U = 0.7Q$.[13b] This difference in core versus valence relaxation is observed in $FeCl_4^-$, which exhibits some Fe 2p core satellite intensity but no off-resonance valence satellite intensity due to its very limited valence relaxation. For the high-spin d^5 core PES peaks, the intensities and energies of the satellites relative to the main lines can be used through a model developed by Sawatzky[13a] to probe the ground-state covalency and define differences in the sulfide relative to the chloride.

Scheme II

g.s.		main PES peak		sat.
↑	→	↑	+	↑↓
↑↓		↓		—

In section III, the variable-energy valence-band PES spectral results for $KFeS_2$ are presented, followed by the core-level Fe 2p spectra for ferric sulfide, which is compared to ferric chloride. In section IV.A, a comparison between the off-resonance and resonance spectra of $FeCl_4^-$ and FeS_4^{5-} is made in order to assign the features in the $KFeS_2$ valence band and determine the ground-state bonding description. In section IV.B, the core level Fe 2p results for both FeS_4^{5-} and $FeCl_4^-$ are analyzed and the parameters obtained from the core-level model are used to compare the ground-state wave functions in these systems. From these studies it is determined that the ground state present in ferric sulfide is inverted as in ferric chloride (Figure 1), with little relaxation on valence ionization, and the covalency in the spin-down levels increases in the sulfide relative to the chloride due to the decreased ionization energy of sulfide relative to chloride valence orbitals. These results are compared to SCF–Xα–SW calculations, and the significance of these results in providing an explanation for the large difference in the optical absorption spectra of mononuclear $FeCl_4^-$ and $Fe(SR)_4^-$ is discussed.

II. Experimental Section

The $KFeS_2$ used in this study was a fibrous, polycrystalline sample and was prepared according to the method of Bronger.[14] The dark purple material crystallizes in a monoclinic space group and consists of infinite chains of edge-sharing D_{2d}-distorted FeS_4 tetrahedra with potassium ions separating the chains. The sample was mounted on an Al stub with UHV compatible Torrseal (Varian Associates) and cleaned in a nitrogen atmosphere by polishing with 9-μm grit Al_2O_3 plastic lapping sheet. After transfer to UHV under N_2, further cleaning was performed by grinding with 100-μm grit diamond particles embedded in a nickel wheel. Purity was checked by the ability to obtain satisfactory valence-band spectra at low photon energies where the cross sections for valence levels of common contaminants are high and by core-level XPS (O 1s, C 1s) prior to use at SSRL.

All XPS data were obtained by using a Vacuum Generators (VG) ESCALAB MkII system using the Mg Kα (1253.6 eV) anode, which was operated at <90 W to minimize radiation damage. The sample was cooled to 160 K, and the pass energy was maintained at 20 eV. All ESCALAB spectra were obtained at normal emission. Details of the ESCALAB system have been described elsewhere.[10] The PES data were obtained by using a Perkin-Elmer PHI system (base pressure of $<1 \times 10^{-10}$ Torr), employing synchrotron radiation at the Stanford Synchrotron Radiation Laboratory (SSRL) on SPEAR beam line III-1, which is equipped with a Grasshopper monochromator.[15] The details of the PHI system have been described elsewhere.[10] Variable-inlet and -exit slits on the monochromator allowed a constant energy resolution of 200 meV to be maintained, and beam-line transmission filters that minimize higher order light contributions to the monochromatic radiation were used up to 70 eV. The pass energy was maintained at 25 eV for all synchrotron PES spectra. Constant initial state (CIS) spectra were obtained by simultaneously scanning the photon energy and analyzed kinetic energy such that the intensity profile of a peak at constant binding energy is generated. The slit widths were adjusted such that the photon energy resolution was always better than 200 meV, and the pass energy was increased to 50 eV to allow greater signal intensity. Constant final state (CFS) spectra, which are equivalent to absorption edges,[16] were obtained with partial yield detection by scanning the photon energy while analyzing 8.0-eV kinetic energy electrons in the secondary tail. The slits and pass energy were set as with CIS. Because of the semiconducting properties of this material, the use of an electron flood gun for charge neutralization was not necessary. All spectra were signal averaged, with 30–40 scans necessary for satisfactory signal to noise. All data taken at SSRL (PES, CIS, CFS) were normalized to the incident photon intensity by a flux monitor that consists of a nickel mesh located in the path of the incident radiation and a total yield channeltron detector.

The details of the ground-state $FeCl_4^-$ spin-unrestricted SCF–Xα–SW calculation used here have been described previously.[1d] The bound-state transition energies were obtained by using the Slater transition-state formalism by transferring 0.5 electrons from the initial orbital to the second orbital of interest and reconverging the potential.[17] Wave functions for these excited states were obtained by transferring 1 electron between the two orbitals and reconverging the potential.

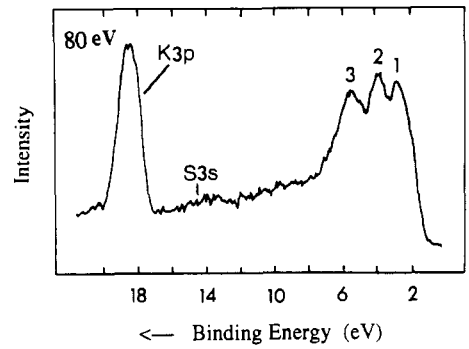

Figure 3. Valence-band PES spectrum of $KFeS_2$ at 80-eV photon energy.

III. Results

The variable photon energy PES spectra of $KFeS_2$ were obtained over the photon energy range 25–100 eV. The complete 80-eV valence-band spectrum is presented in Figure 3. The large peak at 19.0-eV binding energy has been assigned as K 3p, consistent with earlier PES data on $KCuCl_3$.[10] The weak feature at 14.5 eV corresponds to S 3s photoemission, while the three features at lowest binding energy (2–8 eV labeled 1–3) correspond to photoemission from the valence Fe 3d and S 3p levels. All binding energies are referenced to the S 2p core level with a binding energy fixed at 162.8 eV. The variable-energy PES spectra are given in Figure 4 for a wide range of input photon energies. Note that the data in Figure 4 do not have the background subtracted, as the steep background slope makes an estimation of the true base line difficult. The intensity in the region ~7–14 eV is very high at low photon energy and then decreases as the photon energy increases, similar to the intensity behavior expected for C 2p or O 2p, and is also at the correct binding for these impurities. The likely source of this contamination, which could not be removed by scraping in vacuum, is unreacted K_2CO_3 starting material adhering to the polycrystalline sample.[14] However, the low-energy

(12) Manne, R.; Aberg, T. *Chem. Phys. Lett.* **1970**, *7*, 282.
(13) (a) van der Laan, G.; Westra, C.; Haas, C.; Sawatzky, G. A. *Phys. Rev. B: Condens. Matter.* **1981**, *23*, 4369. (b) Zaanen, J.; Westra, C.; Sawatzky, G. A. *Phys. Rev. B: Condens. Matter.* **1986**, *33*, 8060. (c) Park, J.; Ryu, S.; Han, M.-S.; Oh, S.-J. *Phys. Rev. B: Condens. Matter.* **1988**, *37*, 10867.
(14) Bronger, W. *Z. Anorg. Allg. Chem.* **1968**, *359*, 225.
(15) (a) Brown, F. C.; Bachrach, R. Z.; Lien, N. *Nucl. Instrum. Methods* **1978**, *152*, 73. (b) Stohr, J. *Instruction Manual for the New Grasshopper Monochromator*; Stanford Synchrotron Radiation Laboratory: Stanford, CA, 1980. (c) Pate, B. B. Ph.D. Thesis, Stanford University, 1984.
(16) (a) Stohr, J.; Jaeger, R.; Brennan, S. *Surf. Sci.* **1982**, *117*, 503. (b) Hecht, M. Ph.D. Thesis, Stanford University, 1982.
(17) (a) Slater, J. C. *Quantum Theory of Molecules and Solids*; McGraw-Hill: New York, 1974; Vol. 4. (b) Slater, J. C. *Adv. Quantum Chem.* **1972**, *6*, 1.

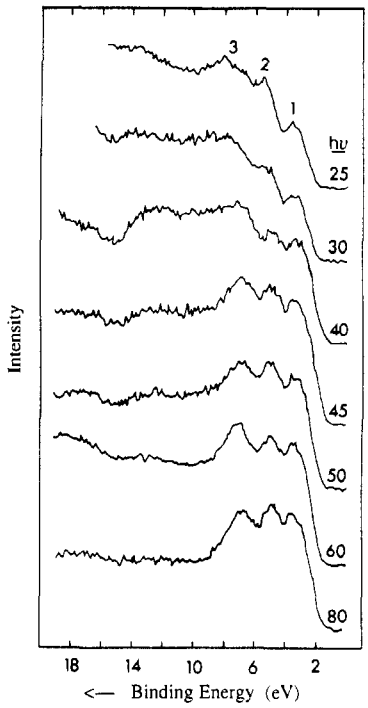

Figure 4. Variable-energy valence-band PES spectra of $KFeS_2$ over the range 25–80 eV.

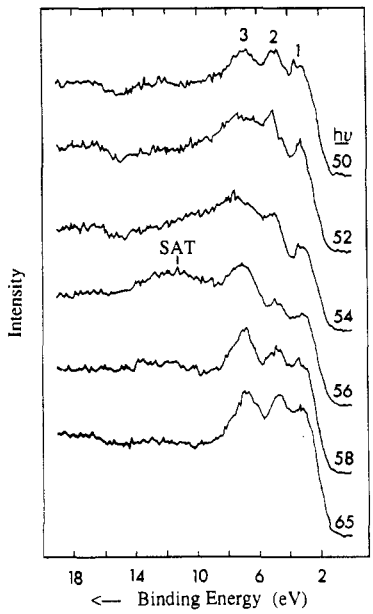

Figure 5. Resonance PES spectra of $KFeS_2$ taken near the Fe 3p absorption edge (56 eV).

region is least affected by the contaminant problem, and qualitative observations may be made. On going from 25 to 30 eV, peak 1 (3.1 eV) shows an increase in intensity relative to peak 2 at 4.5 eV (with little difference in the background). This is indicative of greater metal character in peak 1 relative to peak 2, on the basis of the atomic photoionization cross-section behavior of Fe 3d and S 3p (see Figure 2), and is also observed in $FeCl_4^-$ PES data in ref 1d.

The effects of resonance on the $KFeS_2$ PES spectra were investigated by collecting data with photon energies near the Fe 3p absorption edge. The resonance spectra over the range 50–65 eV are given in Figure 5. The dominant enhancements occur at a photon energy of 56 eV in peak 3 and in the satellite region at ~10-eV binding energy. Although it exhibits resonance, this satellite has negligible off-resonance intensity (Figure 3), similar to our previous results on $FeCl_4^-$. Both peaks 1 and 2 show an initial drop in intensity from 50 to 54 eV, indicating derivative-type antiresonance behavior rather than enhancement. The CIS spectra

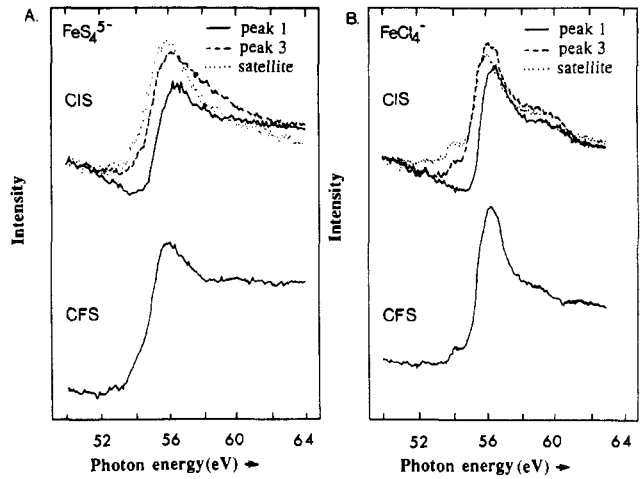

Figure 6. (a) CIS profiles of $KFeS_2$ at the Fe 3p absorption edge for peaks 1 and 3 and the satellite. The CFS edge profile is shown at the bottom for comparison. (b) CIS and CFS profiles of $FeCl_4^-$ at the Fe 3p absorption edge.

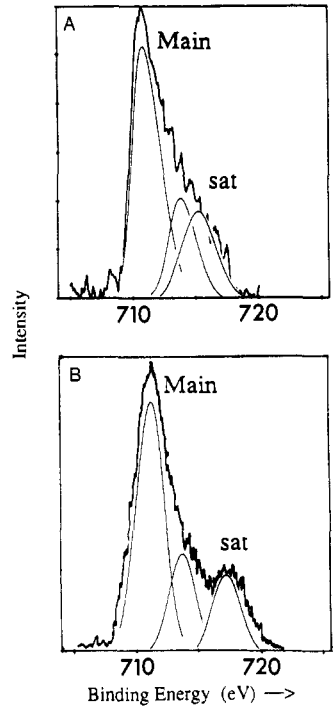

Figure 7. Fe $2p_{3/2}$ core level spectra for (a) FeS_4^{5-} and (b) $FeCl_4^-$.

that show the intensity behavior of each peak as a function of photon energy through resonance are plotted in Figure 6a, along with the CFS absorption edge. As observed in Figure 5, peak 1 exhibits a derivative profile, decreasing in intensity from 50 eV to 54 eV before showing an increase. Both peak 3 and the satellite show enhancement profiles, reaching a maximum in intensity at 56 eV.[18] The CFS absorption edge contains two features: a small peak at 53 eV that has been assigned previously as the $3p^63d^5\ ^6S \rightarrow 3p^53d^6\ ^6D$, ^6F transitions and the main feature at 56 eV, which corresponds to the $3p^63d^5\ ^6S \rightarrow 3p^53d^6\ ^6P$ allowed transition.[19] Comparison between the CIS and CFS shows that the maximum resonance intensity occurs at a photon energy corresponding to the ^6P CFS feature, which confirms that the resonance process involves initial $3p^63d^5\ ^6S \rightarrow 3p^53d^6\ ^6P$ excitation. The CIS and CFS spectra for $FeCl_4^-$ are given in Figure 6b for comparison.[1d] The shapes of the profiles and the intensities are very similar to those of FeS_4^{5-}.

(18) The peak 2 CIS profile showed little resonance, similar to the $FeCl_4^-$ system, and thus is not included.

(19) Bruhn, R.; Schmidt, E.; Schroder, H.; Sonntag, B. *Phys. Lett.* **1982**, *90A*, 41.

Table I. Core-Level XPS Parameters for FeS_4^{5-} and $FeCl_4^-$

	I_s/I_m	ΔE, eV	$2Q/T$	T, eV	Δ, eV	Q, eV	% $\|d^5\rangle$	% $\|d^5L\rangle$
$FeCl_4^-$	0.2	5.3	4	1.4 ± 0.2	3.2 ± 0.5	2.8 ± 0.4	58	35
			5	1.4 ± 0.2	4.5 ± 0.6	3.5 ± 0.5	71	26
			6	1.3 ± 0.2	5.2 ± 0.8	3.9 ± 0.6	75	23
			7	1.3 ± 0.2	6.1 ± 0.9	4.6 ± 0.7	81	18
			8	1.3 ± 0.2	7.0 ± 1	5.2 ± 0.8	84	15
FeS_4^{5-}	0.31	4.2	5	1.1 ± 0.2	1.9 ± 0.4	2.6 ± 0.5	50	41
			6	1.0 ± 0.2	2.9 ± 0.6	3.2 ± 0.6	65	31
			7	1.0 ± 0.2	3.8 ± 0.8	3.7 ± 0.7	74	24
			8	1.1 ± 0.2	5.0 ± 1	4.2 ± 0.8	83	16

The Fe $2p_{3/2}$ core-level XPS for $KFeS_2$ is given in Figure 7a and compared to the $FeCl_4^-$ spectrum in Figure 7b. The $KFeS_2$ Fe 2p spectrum shows a broad, asymmetric peak that tails off to deeper binding energy. Multiplet splitting of the 2p hole is expected to broaden this main peak as in the $FeCl_4^-$. However, the width of the $KFeS_2$ peak is too large and is too intense on the deeper binding energy side to be attributed to multiplet splitting alone. The multiplet splitting was first estimated from the $FeCl_4^-$ spectrum by using a two-peaked gaussian fit to the main line with a third peak in the satellite region. The splitting in the two main peak gaussians was found to be 2.1 eV. In the gaussian analysis of the $KFeS_2$ data, a three-peak fit was also used, fixing the first two gaussians under the main peak at energies consistent with the multiplet splitting in $FeCl_4^-$. The third gaussian in the fit gives the satellite, which contains ~31% of the main-line intensity and is shifted 4.2 eV to deeper binding energy from the average main-line energy. The shake-up satellite peak in the $FeCl_4^-$ spectrum contains only 20% of the main-line intensity and is shifted by 5.3 eV.

IV. Analysis

A. Valence-Band Region. The PES spectra of ferric sulfide exhibit strong similarities to the data[1d] on $FeCl_4^-$, the most obvious of which is the appearance of three peaks in the valence-band region of each spectrum. A comparison with the $FeCl_4^-$ spectrum (at 70-eV photon energy where the contaminant background is less of a problem) provides information on the relative peak energy splittings and intensities. In Figure 8 the peak 1 binding energies have been aligned and normalized to the same intensity and the backgrounds have been subtracted. The energy splittings are very similar, showing only small differences of ≤0.2 eV. In addition, the peak intensities are similar, with the ferric sulfide exhibiting greater peak 3 intensity. This increase in peak 3 intensity indicates somewhat greater Fe 3d character in the levels contributing to peak 3 in FeS_4^{5-} relative to $FeCl_4^-$. The satellite region in $KFeS_2$ is obscured at low photon energy, but at 80 eV (Figure 3), no satellite intensity is detectable in the region 9–12 eV. The lack of off-resonance intensity in the FeS_4^{5-} satellite indicates that little relaxation is occurring in this system on ionization. This result is in agreement with the results[1d] on $FeCl_4^-$, which indicated that the satellite contained <2% of the main-band intensity. The Xα calculations of Taft and Braga are consistent with this lack of relaxation in the ferric sulfide system. They concluded on comparing FeS_4^{5-} and FeS_4^{4-} that the wave functions essentially remain the same on ionization.[20]

From Figure 5, the ferric sulfide exhibits dominant resonance enhancement at 56 eV in peak 3, with significant enhancement in the satellite. This behavior is also the same as observed for ferric chloride. Comparison of the CIS spectra for FeS_4^{5-} and $FeCl_4^-$ in Figure 6 shows enhancement profiles for peak 3 and the satellite but interference profiles for peak 1. From Figures 5 and 6, peak 3 and the satellite in general show greater resonance than peak 1 for both complexes.[21] A more direct comparison of the resonance behavior can be made with the difference curves obtained by subtracting the off-resonance (50 eV) spectrum from the on-resonance (56 eV) spectrum. These difference spectra for (a) $FeCl_4^-$ and (b) FeS_4^{5-} are given in Figure 9 with the peak 1 intensities set equal. The difference spectra clearly exhibit greater resonance enhancement in peak 3 and the satellite for both complexes. The resonance appears to be weaker overall in ferric sulfide, but the spectrum in Figure 9 may be misleading, since it is broad and difficult to estimate the base line.

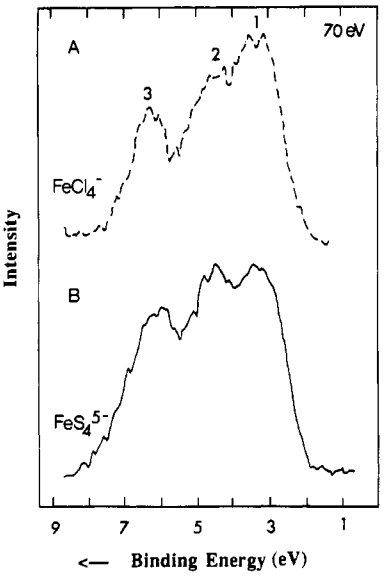

Figure 8. Comparison of the valence-band PES spectra of (a) FeS_4^{5-} and (b) $FeCl_4^-$ at 70-eV photon energy. Spectra are aligned at the peak 1 binding energy and normalized at the peak 1 intensity (energy scale is for FeS_4^{5-}).

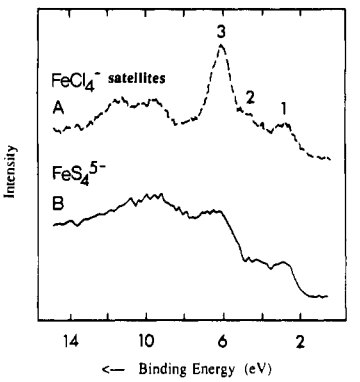

Figure 9. Comparison of the resonance PES difference spectra (56–50 eV) of (a) $FeCl_4^-$ and (b) FeS_4^{5-}. Spectra have been normalized to give equal peak 1 intensities (energy scale is for FeS_4^{5-}).

The above valence-band spectral similarities between the two complexes indicate that the inverted ground-state bonding description found in ferric chloride is also present for ferric sulfide. From Figure 1, peak 1 in the sulfide is assigned as photoemission from the dominantly S 3p spin-up antibonding levels, with a contribution from S 3p nonbonding. Peak 2 contains the remainder of the S 3p nonbonding contribution along with the S 3p spin-down bonding levels, and peak 3 is assigned as photoemission from the dominantly Fe 3d bonding spin-up levels. The

(20) Taft, C. A.; Braga, M. *Phys. Rev. B: Condens. Matter.* **1983**, *28*, 7308.
(21) The CIS profiles reflect the intensity at a specific binding energy and not the total integrated intensity of a peak. The profile is thus subject to variations due to the binding energy chosen and charging effects and cannot be used quantitatively.

greater peak 3 intensity in $KFeS_2$ is indicative of greater metal character, and thus a decrease in covalency, in the Fe 3d spin-up bonding levels.

B. Core Levels. While the lack of valence shake-up intensity indicates little relaxation, the core spectrum does show shake-up intensity (Figure 7), which indicates some relaxation is occurring for core ionization. Analysis of the core-level data allows an estimate of the core relaxation caused by the additional presence of the metal ion 2p–3d Coulomb interaction, Q. Table I gives values for the main-line satellite splitting (ΔE) and the satellite to main peak (I_s/I_m) intensity ratio for ferric sulfide and chloride. In $KFeS_2$, the satellite is closer to the main line in energy by $\sim$1 eV and contains 31% of the main-line intensity compared to 20% in $FeCl_4^-$. Physical insight into these differences can be obtained from application of a multivalence hole model developed by Park[13c] as an extension of an earlier model by Sawatzky.[13a,b] The ground state is treated as a mixture of the $|d^5\rangle$ configuration with the "charge-transfer" states $|d^6L\rangle$, $|d^7L^2\rangle$, $|d^8L^3\rangle$, $|d^9L^4\rangle$, and $|d^{10}L^5\rangle$, where L denotes a hole on the ligand. The diagonal matrix elements are

$$\begin{aligned}
\langle d^5|H|d^5\rangle &= 0 \text{ (reference)} \\
\langle d^6L|H|d^6L\rangle &= \Delta \\
\langle d^7L^2|H|d^7L^2\rangle &= 2\Delta + U \\
\langle d^8L^3|H|d^8L^3\rangle &= 3\Delta + 2U \\
\langle d^9L^4|H|d^9L^4\rangle &= 4\Delta + 3U \\
\langle d^{10}L^5|H|d^{10}L^5\rangle &= 5\Delta + 4U
\end{aligned} \tag{1}$$

where Δ is the charge-transfer energy, $\Delta = E(d^6L) - E(d^5)$, and U is the metal 3d–3d Coulomb repulsion. The covalent mixing matrix element, T, is defined as

$$T = \langle d|H|L\rangle \tag{2}$$

and is approximated as being the same for e and t_2 orbitals, and thus the $10D_q$ splitting is also ignored. The off-diagonal elements are

$$\begin{aligned}
\langle d^5|H|d^6L\rangle &= \sqrt{5}T \\
\langle d^6L|H|d^7L^2\rangle &= \sqrt{8}T \\
\langle d^7L^2|H|d^8L^3\rangle &= 3T \\
\langle d^8L^3|H|d^9L^4\rangle &= \sqrt{8}T \\
\langle d^9L^4|H|d^{10}L^5\rangle &= \sqrt{5}T
\end{aligned} \tag{3}$$

All other off-diagonal elements are zero. Diagonalization of this 6×6 matrix gives a ground-state wave function that can be written

$$\Psi_g = a|d^5\rangle + b|d^6L\rangle + c|d^7L^2\rangle + d|d^8L^3\rangle + e|d^9L^4\rangle + f|d^{10}L^5\rangle \tag{4}$$

with $|a|^2 + |b|^2 + |c|^2 + |d|^2 + |e|^2 + |f|^2 = 1$.

Ionization creates a core hole on the metal that shifts the metal 3d levels to deeper binding energy due to the 2p hole–3d electron Coulomb attraction. The diagonal elements for the final state become

$$\begin{aligned}
\langle cd^5|H|cd^5\rangle &= E_c \\
\langle cd^5L|H|cd^6L\rangle &= E_c + \Delta - Q \\
\langle cd^7L^2|H|cd^7L^2\rangle &= E_c + 2(\Delta - Q) + U \\
\langle cd^8L^3|H|cd^8L^3\rangle &= E_c + 3(\Delta - Q) + 2U \\
\langle cd^9L^4|H|cd^9L^4\rangle &= E_c + 4(\Delta - Q) + 3U \\
\langle cd^{10}L^5|H|cd^{10}L^5\rangle &= E_c + 5(\Delta - Q) + 4U
\end{aligned} \tag{5}$$

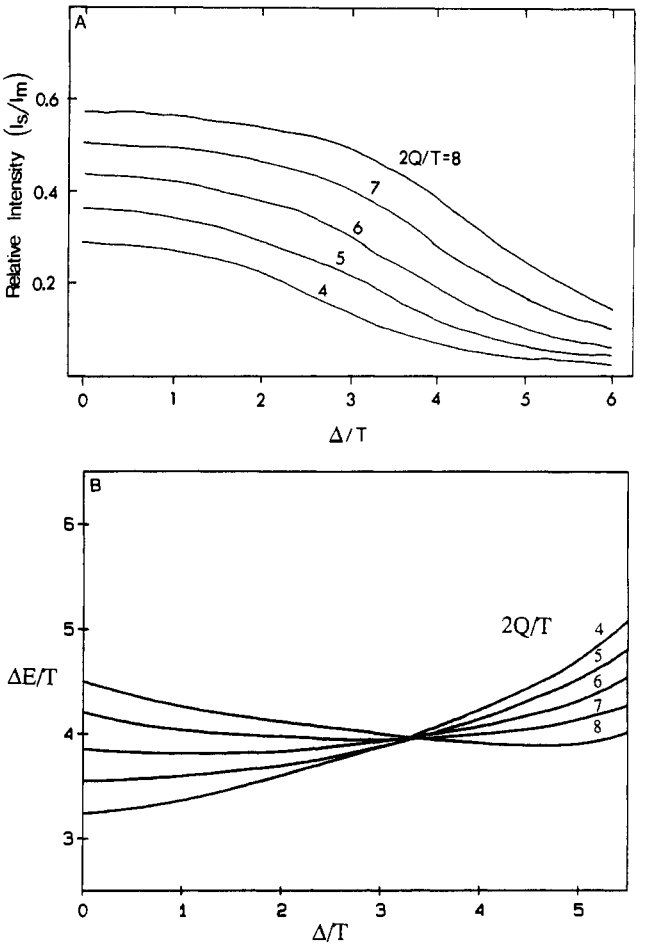

Figure 10. Theoretical curves for d^5 complexes for the first core satellite as a function of Δ/T for $2Q/T$ = 4, 5, 6, 7, and 8: (a) relative intensities of satellites to main line; (b) main-line–satellite energy differences in units of T. Adapted from ref 13c.

where E_c is the energy of the core hole. The off-diagonal elements are treated as being the same as in the ground state (eq 3). Solving the matrix with eqs 3 and 5 gives the final-state wave functions Ψ_i, i = 1–6. In principle, the final-state spectrum should exhibit one main line (d^5) and five satellites; however, only the first satellite (d^6L) is observed in our data. The XPS intensity is calculated by applying the sudden approximation:

$$\Psi_R(N-1) = \sum_{i=1}^{6} \langle \Psi_i|\Psi_R\rangle \Psi_i(N-1) \tag{6}$$

where the frozen-orbital final states are expanded in terms of the relaxed final states. $\Psi_R(N-1)$ is the remainder wave function of the frozen-orbital state after one-electron ionization, and the $\Psi_i(N-1)$ are the ground and excited states of the relaxed ion. The relative cross sections of these relaxed states are given by the square of the overlap integral in eq 6.

Thus, the intensities of core-level peaks can be obtained by using eq 6 and the energies from eqs 3 and 5. These energies and intensities will vary with Δ, T, U, and Q. Estimates for these parameters can be made by plotting the two experimental observables (ΔE and I_s/I_m) as a function of Δ, T, U, and Q. All energies are in units of T, and the approximation is made that $U/Q = 0.7$.[13b] The resulting curves for the first satellite are reproduced in Figure 10a,b. Since for each complex there are only two experimental observables (I_s/I_m and ΔE), it is not possible to solve for all three parameters (Δ, T, and Q). However, for a given value of Q, values of Δ and T can be determined. Q should be reasonably independent of ligand and thus approximately the same for both the sulfide and chloride complexes. From Figure 10a and the relative intensities of the satellites in FeS_4^{5-} and $FeCl_4^-$ of 0.31 and 0.20, respectively (Table I), a set of values for Δ/T

Table II. Initial-State Spin-Unrestricted Xα–SW Wave Functions

level		$FeCl_4^-$ [a] % Fe	$FeCl_4^-$ [a] % Cl	FeS_4^{5-} [b] % Fe	FeS_4^{5-} [b] % S
$5t_2\downarrow$		74	26	59	18
$2e\downarrow$	unocc	80	20	75	9
$5t_2\uparrow$		36	64	21	44
$2e\uparrow$		21	79	17	40
$3t_2\downarrow$		31	69	7	37
$1e\downarrow$		20	80	17	37
$3t_2\uparrow$		65	35	75	12
$1e\uparrow$		79	21	78	8

[a] Taken from ref 1d. [b] Taken from ref 4.

Table III. Experimental Transition Energies (cm^{-1}) for $FeCl_4^-$ and $Fe(SR)_4^-$

transition	$FeCl_4^-$ [a]	$Fe(SR)_4^-$ [b]	transition	$FeCl_4^-$ [a]	$Fe(SR)_4^-$ [b]
$^4T_1$, $^4T_2$ (av)	14780	8420	$^6T_2$	27300	12970
^4E	18200	11230			

[a] Taken from ref 1c. [b] Taken from ref 1a,b.

are found for possible values of $2Q/T$. From these Δ/T values with Figure 10b, the values of $\Delta E/T$ are obtained. This leads to a determination of T and Δ values for each possible value of $2Q/T$, which are listed in Table I. Comparison of the values obtained for the two complexes for similar values of Q indicates that the major difference is in the value of Δ, which is always about 1 eV smaller for the sulfide. The experimentally determined values of Δ, T, Q, and U ($=0.7Q$) have been included in the matrix described by eqs 1 and 3 to give the ground-state wave function (Table I, % $|d^5\rangle$ and % $|d^6\underline{L}\rangle$). The wave functions obtained, for fixed Q, show that the FeS_4^{5-} ground state is generally more covalent, which is mostly due to the reduced value of Δ. Note that the values of Δ and the ground-state wave functions obtained from the core analysis apply to the spin-down levels in the spin-unrestricted bonding scheme in Figure 1, as the charge-transfer transitions involved in the shake-up occur between these spin-down levels.

V. Discussion

The results of this study indicate that the ground-state bonding description in high-spin tetrahedral ferric sulfide is analogous to that of ferric chloride in Figure 1, which is inverted from the usual ordering found in transition-metal complexes. The ferric sulfide PES data are very similar to the ferric chloride data: both complexes exhibit three peaks in the valence-band spectrum with similar energy splittings and intensity ratios, as well as dominant resonance enhancement in peak 3 at the Fe 3p absorption edge. In addition, neither complex shows evidence for relaxation on ionization. Comparison of the 70-eV spectra for both complexes shows that the sulfide salt has a larger peak 3 intensity relative to that of peak 1 than the chloride salt, indicating greater metal character in the sulfide spin-up bonding levels, and thus decreased spin-up covalent mixing. Alternatively, analysis of the shake-up energy decrease and intensity increase of the sulfide shows the spin-down levels are more covalent in the sulfide. These differences in covalent mixing are due to the difference in experimental Δ values ($\delta\Delta = \Delta(FeCl_4^-) - \Delta(FeS_4^{5-})$) of $\sim$1 eV found from the core analysis, which reflects the lower ionization energy of sulfide relative to the chloride. This shifts the ligand levels (L 3p) in Figure 1 closer to the $3d\downarrow$ but further from the Fe $3d\uparrow$ levels. This increase in spin-down covalency and decrease in spin-up covalency for FeS_4^{5-} relative to $FeCl_4^-$ is reproduced by spin-unrestricted Xα–SW calculations of their ground state as summarized in Table II.

While the basic bonding description of ferric sulfide is the same as that for ferric chloride, large differences are observed on comparison of the optical absorption spectra of ferric chloride and ferric tetrathiolate.[1a-c] The energies of three representative transitions for both $FeCl_4^-$ and $Fe(SR)_4^-$ are listed in Table III.

Table IV. Xα–SW Calculated Transition Energies (cm^{-1}) for $FeCl_4^-$, $Fe(SR)_4^-$, and FeS_4^{5-}

transition	$FeCl_4^-$	$Fe(SR)_4^-$ [a]	FeS_4^{5-} [b]
$^4T_1$, $^4T_2$ (av)	15920	9450	
$^6T_2$	26900	13400	12950

[a] Taken from ref 2a. [b] Taken from ref 6.

The lowest energy $^6A_1 \rightarrow {}^4T_1$ and $^4T_2$ spin-forbidden transitions correspond to excitation of an antibonding $5t_2\uparrow$ electron to the antibonding $2e\downarrow$ orbital and thus would be considered a d → d transition in ligand field theory (LFT).[22] The spin-forbidden $^6A_1 \rightarrow {}^4E$ corresponds to a spin-flip of an electron in the antibonding t_2 level ($5t_2\uparrow \rightarrow 5t_2\downarrow$) and is also considered a d → d transition in LFT. The lowest energy spin-allowed $^6A_1 \rightarrow {}^6T_2$ involves excitation of a ligand nonbonding $t_1\downarrow$ electron to the antibonding $2e\downarrow$ orbital and thus corresponds to a ligand-to-metal charge-transfer transition in LFT. From Table III, the change in ligand from chloride to thiolate (and sulfide[6]) causes a very large decrease in these transition energies. The change in ligand is expected to have a large effect on ligand-to-metal charge-transfer energies, reducing them by approximately the decrease in ligand ionization energy, $\delta\Delta$, which we find to be on the order of 1 eV for sulfide relative to chloride. Experimentally, the charge-transfer decrease is 14300 cm^{-1}. However, the effect on d → d energies would be expected to be much smaller, with some decrease in energy due to relatively limited changes in $10D_q$ and covalent decrease of valence electron repulsion. However, the energies given in Table III indicate that the LFT assigned d → d transitions ($^6A_1 \rightarrow {}^4T_1$, $^4T_2$, ^4E) are strongly affected, with the average $^4T_1$, $^4T_2$ energy dropping from 14780 cm^{-1} in the chloride to 8420 cm^{-1} in the thiolate. In LFT the $^6A_1 \rightarrow {}^4E$ spin-flip transition ($5t_2\uparrow \rightarrow 5t_2\downarrow$) is independent of D_q; therefore, its lower energy would only reflect a reduction in electron repulsion due to covalency (i.e. a nephelauxetic effect[23]). The observed decrease of 7000 cm^{-1} from Table III for these high-spin ferric complexes can be contrasted, for example, to the relatively limited change of 1900 cm^{-1} observed[24] for the $^4A_{2g} \rightarrow {}^2E_g$ ligand field transition in d^3 Cr^{3+} in going from chloride to thiolate ligation. An attempt to fit the ferric thiolate $^4T_1$, $^4T_2$, and ^4E transitions to a ligand field model results in an absurdly small value of the Racah electron repulsion parameter B = 22 cm^{-1} (B(free Fe^{3+} ion) = 1100 cm^{-1}).

Alternatively, we have performed transition-state Xα calculations on these spin-forbidden transitions and the spin-allowed $^6T_2$ transition in $FeCl_4^-$. The results are listed in Table IV along with those calculated earlier for the thiolate and sulfide for comparison to the experimental energies in Table III. These Xα calculations, which show similar ground states for the chloride and thiolate, reproduce the large changes in spin-forbidden and charge-transfer transition energies very well. A closer look at the spin-unrestricted Xα results for the chloride provides insight into the origin of this extreme reduction in the energies of these transitions. From Figure 1, the spin-allowed transitions $L^{nb}\downarrow \rightarrow Fe^{ab}\downarrow$ are still described as ligand-to-metal charge transfer and should shift to lower energy by $\delta\Delta \sim 1$ eV. As indicated earlier, the spin-forbidden $^6A_1 \rightarrow {}^4T_1$ and $^4T_2$ bands arise from the antibonding $t_2\uparrow \rightarrow$ antibonding $e\downarrow$ transition and would normally be viewed as "d → d" transitions in LFT. However, the spin-unrestricted Xα wave function for the spin-up antibonding $t_2\uparrow$ ($L^{ab}\uparrow$) contains mostly ligand character for both ferric chloride and ferric thiolate complexes, while the unoccupied $e\downarrow$ and $t_2\downarrow$ levels ($Fe^{ab}\downarrow$) have mostly metal character (Table II). Therefore, the spin-unrestricted energy level diagram in Figure 1 describes the transition as a ligand-to-metal charge-transfer process. The same is true for the $5t_2\uparrow \rightarrow 5t_2\downarrow$ spin-flip ^4E transition. This Xα description is consistent with the fact that

(22) The Xα–SW formalism does not distinguish between the $^4T_1$ and $^4T_2$ components of the $5t_2\uparrow \rightarrow 2e\downarrow$ transition—only the weighted average energy can be obtained. The experimental energies are thus reported as the average for comparison to the Xα–SW values.

(23) Ferguson, J. *Prog. Inorg. Chem.* **1970**, *12*, 159.
(24) Jørgensen, C. K. *Prog. Inorg. Chem.* **1962**, *4*, 73.

Table V. Xα–SW Excited-State Wave Functions for $FeCl_4^-$

level		ground state		$^4T_{1,2}(5t_2\uparrow \rightarrow 2e\downarrow)$		$^4E(5t_2\uparrow \rightarrow 5t_2\downarrow)$		$^6T_2(1t_1\downarrow \rightarrow 2e\downarrow)$	
		% Fe	% Cl	% Fe	% Cl	% Fe	% Cl	% Fe	% Cl
$5t_2\downarrow$		74	26	80	20	80	20	85	15
$2e\downarrow$	unocc	80	20	83	17	82	18	90	10
$5t_2\uparrow$	occ	36	64	55	45	53	47	72	28
$2e\uparrow$		21	79	50	50	45	55	70	30
$4t_2\downarrow$		11	89	10	90	10	90	11	89
$4t_2\uparrow$		17	83	15	85	16	84	7	93
$3t_2\downarrow$		31	69	30	70	30	70	76	24
$1e\downarrow$		20	80	17	83	18	82	10	90
$3t_2\uparrow$		65	35	48	52	50	50	36	64
$1e\uparrow$		79	12	50	50	55	45	30	70
Δq				+0.22	−0.22	+0.20	−0.20	+0.41	−0.41

a large decrease in energy is observed for all the transitions in Table III and not just the $^6T_2$ spin-allowed charge transfer, when the ligand is changed, since from Figure 1 all the above transitions would involve ligand-to-metal charge transfer and hence be strongly affected by $\delta\Delta$.

However, the ground-state spin-polarized energy level diagram for high-spin d^5 in Figure 1 does not provide a complete description of the transitions: large relaxation changes can occur in the wave functions upon bound-state excitation. The wave functions for the $^4T_{1,2}$, ^4E, and $^6T_2$ excited final states of ferric chloride are compared to the ground-state wave functions in Table V. For all excitations, the spin-up $5t_2\uparrow$, $2e\uparrow$ antibonding levels, which have mostly ligand character in the ground state, become mostly metal on excitation. The spin-up $3t_2\uparrow$, $1e\uparrow$ metal bonding levels change to mostly ligand. Thus, population of the Fe $3d\downarrow$ levels in the excited state substantially lowers the exchange interaction relative to the ground state, resulting in a large relaxation that changes the energy of the Fe $3d\uparrow$ levels. In order to quantitate the net charge transfer including relaxation in the bound-state transitions, the charge redistribution, Δq, accompanying excitation was calculated for the $FeCl_4^-$ system by summing eq 7 over all occupied valence levels, i:

$$\Delta q_i = \sum_i (q(\text{final state}) - q(\text{ground state})) \qquad (7)$$

where q are the coefficients from Table V weighted by the orbital occupancy. The resulting Δq's for each transition are included at the bottom of Table V. The spin-allowed $^6T_2$ charge transfer shows 0.4 of an electron shifted, while the spin-forbidden transitions show 0.2 electron transferred.[25] While some charge redistribution is expected for a "d → d" transition due to covalency differences in the d orbitals, the value of 0.2 electron is large, being half that of the spin-allowed ligand-to-metal charge-transfer transition. Thus, the lowest energy spin-forbidden transitions normally described as d → d contain a great deal of charge-transfer character. The spin-forbidden $^4T_1$, $^4T_2$, and ^4E transitions are decreased in energy by half that observed for the spin-allowed charge transfer on going from the chloride to the thiolate, consistent with the relative amounts of charge-transfer character predicted for these transitions.

The nature of the spin-forbidden transitions in high-spin d^5 complexes is strongly complicated by spin-polarization effects in the initial state and large relaxation effects in the excited states due to the change in spin polarization. These effects cause what would normally be considered d → d transitions in LFT to obtain a great deal of charge-transfer character, about half that of a normal charge-transfer transition. The experimental evidence for this is the large shift in the energies of the spin-forbidden transitions in the thiolate relative to the chloride, a shift that is too large for the ligand field description, as this would require an unreasonable reduction in electron repulsion, but is reproduced by Xα calculations that include spin polarization.[26,27]

Acknowledgment. We thank the Stanford Synchrotron Radiation Laboratory (SSRL), which is supported by the U.S. Department of Energy, for providing beam time, the Stanford Center for Materials Research, which is supported by the Division of Materials Research of the National Science Foundation, for providing experimental facilities, Yujo Ito for providing the $KFeS_2$ crystals, Stephen Didziulus for experimental assistance, and the National Science Foundation (Grant No. CHE-8613376) for financial support of this research.

Registry No. FeS_4^{5-}, 56509-84-3; $FeCl_4^-$, 14946-92-0; $KFeS_2$, 12022-42-3; Fe, 7439-89-6.

(25) This same value of 0.2 was also found for the high-energy spin-forbidden $Fe^{b}\uparrow$ bonding to $Fe^{ab}\downarrow$ antibonding transitions in Figure 4-1.

(26) Note that He I and He II photoelectron spectra[29,30] and spin-unrestricted Xα–SW calculations[29] on triatomic $MnCl_2$ indicate that the ground state of this high-spin Mn^{2+} complex is inverted. However, unlike Fe^{3+} the spin-forbidden $^6A_1 \rightarrow {}^4E$ transition in Mn^{2+} complexes is relatively insensitive[24] to changes in ligand (for Cl^- to S^{2-}, the ^4E shifts by only 1450 cm^{-1}). For Mn^{2+} the lowest energy spin-allowed charge-transfer transition is about 20000 cm^{-1} higher in energy than in the corresponding Fe^{3+} complexes, indicating that the Mn^{2+} 3d levels are at much lower binding energy. This lower binding energy coupled with the lower exchange splittings in the $^4\Gamma$ bound final states favors a more normal ligand field description of the $^4\Gamma$ states in Mn^{2+} complexes. Alternatively, photoionization relaxation increases the Mn^{2+} 3d binding energy resulting in an enhancement of the inverted bonding description as is observed in the PES data.

(27) The charge-transfer nature of the spin-forbidden transitions is also reflected in their 10-fold increase in intensity in the T_d $FeCl_4^-$ complex relative to the isoelectronic T_d $MnCl_4^{2-}$ complex.[1,31]

(28) (a) Tossell, T. A.; Urch, D. S.; Vaughan, D. J.; Wierch, G. *J. Chem. Phys.* **1982**, *77*, 77. (b) Hamajima, T.; Kambra, T.; Gondaira, K. I.; Oguchi, T. *Phys. Rev. B* **1981**, *24*, 3349.

(29) MacNaughton, R. M.; Bloor, J. E.; Sherrod, R. E.; Schweitzer, G. K. *J. Electron Spectrosc. Relat. Phenom.* **1981**, *22*, 1.

(30) Lee, E. P. F.; Potts, W. A.; Doran, M.; Hillier, I. H.; Delaney, J. J.; Hawksworth, R. G. *J. Chem. Soc., Faraday Trans. 2* **1980**, 506.

(31) Furlani, C.; Furlani, A. *J. Inorg. Nucl. Chem.* **1961**, *19*, 51.